# Suppression of Real Power Back Flow of Nonregenerative Cascaded H-Bridge Inverters Operating Under Faulty Conditions

Le Sun, *Student Member, IEEE*, Zhenxing Wu, Fei Xiao, Xinjian Cai, and Shuxiu Wang

***Abstract*—When the faulty cells of a nonregenerative cascaded H-bridge inverter are bypassed, it is necessary to inject a zero-sequence voltage into the inverter phase voltages so as to achieve the maximum balanced line-to-line voltage. However, the injected zero-sequence voltage may lead to a back flow of real power (BFRP) in at least one phase so that the dc voltage will rise to an intolerable level. To solve the problem, this paper proposes a new method of generating zero-sequence voltages. This method can not only maximize the available output voltage but also suppress the BFRP effectively. The zero-sequence voltage is always limited to an appropriate range to achieve the maximum output voltage through linear modulation. Closed-loop control is used to minimize the fundamental component of the zero-sequence voltage so that the power is less likely to flow back. Compared with the conventional methods, the proposed method allows the inverter to drive a load with a lower power factor not inducing BFRP or degrading the output voltage capability. As a result, the probability of overvoltage on the dc side is reduced. The experimental results show that the proposed method is effective and feasible.**

***Index Terms*—Cascaded H-bridge (CHB) inverter, fault tolerant, modulation, real power back flow, zero sequence.**

## I. Introduction

MULTILEVEL inverters have attracted much attention in recent years [1], [2]. The topologies of multilevel inverters mainly include diode-clamped inverters [3], flying-capacitor inverters [4], cascaded H-bridge (CHB) inverters [5], and modular multilevel converters [6]. Among them, CHB inverters have been widely used for high-voltage motor drives due to their good power quality [7]. Fig. 1 shows a typical CHB inverter. Owing to the large number of power cells, its failure probability is comparatively high. Therefore, the reliability of CHB inverters has been the focus of a great deal of research [8]–[10]. On the other hand, when one or several cells of a CHB inverter fail, these faulty cells can be short-circuited by bidirectional thyristors [11] or bypass contactors [12], and the inverter can continue its operation. Such fault-tolerant operation needs both accurate fault diagnosis and appropriate control methods under fault conditions [13]. Much work has been done on the former [11], [14], [15], while this paper focuses on the latter.

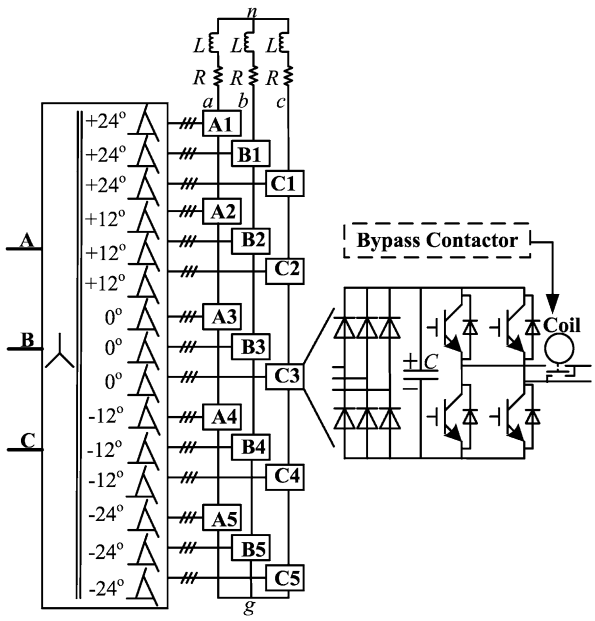


Fig. 1. CHB inverter.

After the faulty cells are isolated, there may be a difference in the number of the remaining normal cells in three phases, so the maximum available output voltages in three phases also may be different. If the modulating signals are not adjusted accordingly, the output line-to-line voltages may be unbalanced. To solve the problem, several fault-tolerant methods have been proposed, which include using redundant cells, adjusting dc voltages, bypassing the cells at the same level, using redundant switching states, and injecting a zero-sequence voltage.

Using redundant cells is a hardware method, which means that an extra cell must be added in each phase besides the cells required for normal operation [16]. With redundant cells, the inverter can tolerate at least one faulty cell with no loss of capacity. However, the redundant cells inevitably increase cost. The method based on the adjustment of dc voltages is to raise the dc voltages of the remaining cells in the faulty phases [17].

Manuscript received April 24, 2015; revised July 18, 2015; accepted August 28, 2015. Date of publication September 10, 2015; date of current version January 28, 2016. This work was supported by the National Natural Science Foundation of China under Grant 51490681 and the National High Technology Research and Development Program (863 Program) of China under Project 2013AA050404. This paper was presented in part at the 6th Annual IEEE Energy Conversion Congress and Exposition, Pittsburgh, PA, USA, September 15–18, 2014. Recommended for publication by Associate Editor B. Choi.

L. Sun is with the School of Electrical Engineering, Xi'an Jiaotong University, Xi'an 710049, China, and also with the Ship Integrated Power Technology Key Laboratory, Naval University of Engineering, Wuhan 430033, China (e-mail: le_sunjt@163.com).

Z. Wu, F. Xiao, X. Cai, and S. Wang are with the Ship Integrated Power Technology Key Laboratory, Naval University of Engineering, Wuhan 430033, China (e-mail: 40999794@163.com; 24500401@qq.com; 33438059@qq.com; wangshuxiu1944@163.com).

Color versions of one or more of the figures in this paper are available online at http://ieeexplore.ieee.org.

Digital Object Identifier 10.1109/TPEL.2015.2477849

This method enables the inverter to keep its normal output voltage capability under fault conditions, but it can be used only in the applications in which dc voltages are controllable, such as static var compensators (STATCOM) and CHB inverters with front-end PWM rectifiers providing dc voltages. Moreover, the switching devices are required to endure a voltage higher than the normal level, which also increases cost. The method based on bypassing the cells at the same level means bypassing an equal number of cells in all three phases, even if some of these bypassed cells have not failed [13]. This method bypasses too many normal cells, so the output voltage capability will drop severely, especially when the majority of the faulty cells are concentrated in one phase. Redundant switching states are generally used in the space vector pulse width modulation [18]. Because a CHB inverter has many switching states, the complexity of the methods based on redundant switching states increases significantly with increasing number of cells.

Injecting a zero-sequence voltage may be the most practical fault-tolerant method. Among all, the methods based on zero-sequence voltage injection, the neutral point shift (NPS) method may be the earliest one [19]. This method bypasses only the faulty cells and balances the line-to-line voltages by adjusting the amplitude and phase of the inverter phase voltages. The essence of the NPS method is to inject a fundamental zero-sequence voltage. The maximum available output voltage achieved by the NPS method is higher than that achieved by bypassing the cells at the same level. However, the NPS method requires that the ratio of the amplitude values of the three-phase inverter voltages should be the same as the ratio of the numbers of the remaining normal cells in three phases. Limited by this, the output voltage capability of the CHB inverter cannot be fully raised. In [20], the NPS method is improved by forcing the phase angle between the two inverter phase voltages with the lowest amplitude values to be 180°. However, this method can extend the output voltage capability only under some special fault conditions. In [21], the amplitude and phase of the inverter phase voltages are not directly changed; instead, a zero-sequence voltage generated by the closed-loop control is injected. This method can fully raise the output voltage capability under all fault conditions apart from the case when all cells in one phase are bypassed. In [22] and [23], open-loop methods are used to generate the zero-sequence voltage. Among all, these methods based on zero-sequence voltage injection, it can be verified that, under most fault conditions, the methods proposed in [21] and [22] are capable of achieving higher output voltage through linear modulation than the other methods.

However, these methods have two common problems. One problem is that the input power quality and the output power quality may be degraded when several cells are bypassed [21]. In spite of this, this is often acceptable compared with a complete shutdown, as pointed out in [21]. The other problem is that the injected zero-sequence voltage may interact with the output currents and produce negative real power in at least one phase. This problem is more serious. If the negative power from the zero-sequence voltage is greater than the positive power from the positive-sequence voltage, the back flow of real power (BFRP) will occur. For those CHB inverters which are capable of regeneration, the real power can be returned to the grid [24]. Unfortunately, many CHB inverters have a topology as shown in Fig. 1, where diode rectifiers are used to provide dc voltages. These inverters cannot return the real power to the grid. Thus, when the real power flows back to the dc side, the dc voltages will rise to an intolerable level, and, finally, damage the inverters. Moreover, the lower the load power factor (PF), the more likely the real power is to flow back [21].

To solve this problem, Hammond [21] suggests reducing the motor voltage to keep the load PF high enough at light load. This will weaken the flux of the motor. Although weakening flux helps to save energy at light load, it may degrade the maximum output torque and the ability to resist disturbances [25]. Therefore, the flux is kept at a high level in most applications. Moreover, energy saving effects of weakening the flux is not significant if the light-load operation time is not long. In addition, it is difficult to know exactly how high the load PF should be to avoid BFRP. Instead of changing load PF, Lezana [20] improves the modulation method under fault conditions to enable the inverter to tolerate lower load PF. However, as mentioned previously, this method can improve the NPS method only in some special fault conditions. Except [20] and [21], little literature is available on the issue of BFRP under fault conditions.

Since BFRP results from the injected zero-sequence voltage, we may avoid it by controlling the zero-sequence voltage. Injecting zero-sequence voltage to balance three-phase power is not a new idea. In [26], it is used to solve the power unbalance problem caused by negative-sequence currents. It is also adopted in [27] for balancing dc voltages in CHB STATCOMs, and in [28] and [29] for balancing SOC in CHB battery energy storage systems. However, these methods do not consider the requirement for the zero-sequence voltage to maximize output voltage capability without overmodulation. When CHB inverters operate under fault conditions, this requirement is important.

This paper proposes a new method of generating the zero-sequence voltage. The method can effectively suppress BFRP by reducing the fundamental component of the zero-sequence voltage. Moreover, the generated zero-sequence voltage is always limited to an appropriate range so that the amplitude of the output voltage can be raised to the maximum level without overmodulation. As a result, the proposed method can not only successfully maximize the output voltage capability but also extend the allowable range of the load PF under fault conditions. The organization of this paper is as follows. Section II investigates the requirements for the zero-sequence voltage in terms of maximizing available output voltage and suppressing BFRP. In Section III, the principle and the implementation of the proposed method are explained in detail. In Section IV, experimental results are provided to verify the validity of the proposed method. Finally, the paper is concluded in Section V.

## II. Requirements for the Zero-Sequence Voltages

Fig. 2 shows the basic block diagram of the modulation method based on zero-sequence voltage injection. In Fig. 2, $u_{an}$, $u_{bn}$, and $u_{cn}$ are the reference voltages; $u_0$ is the zero-sequence voltage; $u_{ag}$, $u_{bg}$, and $u_{cg}$ are the modulating voltages; $u^*_{ag}$, $u^*_{bg}$,

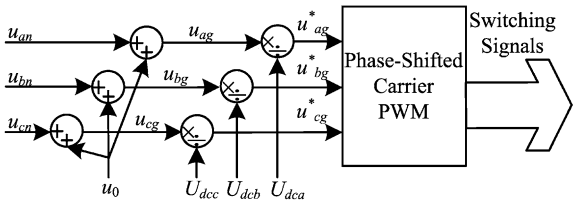


Fig. 2. Basic block diagram of the modulation method based on zero-sequence voltage injection.

and $u^*_{cg}$ are the normalized modulating signals; and $U_{\mathrm{dc}a}, U_{\mathrm{dc}b}$, and $U_{\mathrm{dcc}}$ are the sums of the dc voltages of the normal cells in each phase. In this paper, $U_{\mathrm{dc}a}, U_{\mathrm{dc}b}$, and $U_{\mathrm{dcc}}$ are called available dc voltages in phases *a*, *b*, and *c*, respectively. Suppose that the dc voltage of each cell is $V_{\mathrm{dc,cell}}$ and the numbers of the normal cells in phases *a*, *b*, and *c* are $N_a, N_b$, and $N_c$, respectively. Then, we have $(U_{\mathrm{dc}a}, U_{\mathrm{dc}b}, U_{\mathrm{dcc}}) = (N_a, N_b, N_c)$ $V_{\mathrm{dc,cell}}$. Different sets of $(N_a, N_b, N_c)$ represent different fault conditions.

In this paper, high-frequency harmonics caused by PWM are ignored. Thus, within the linear modulation region, $u_{an}, u_{bn}$, and $u_{cn}$ are also the load phase voltages between the output terminals *a*, *b*, or *c* and the load neutral point *n* in Fig. 1; $u_{ag}, u_{bg}$, and $u_{cg}$ are also the inverter phase voltages between the output terminals *a*, *b*, or *c* and the inverter neutral point *g* in Fig. 1.

The requirements for $u_0$ include two aspects: not degrading the output voltage capability and not leading to BFRP.

### *A. Requirement for the Zero-Sequence Voltage to Maximize the Output Voltage Capability*

In this paper, subscript *k* represents the phase and can be *a*, *b*, or *c*. Suppose that the reference voltage in phase *k* is

$$u_{kn} = U_{m,\mathrm{phase}}\sin(\omega t + \varphi_k), k \in \{a, b, c\} \tag{1}$$

where $\varphi_k$ equals 0, $-2\pi/3$, or $2\pi/3$ when *k* is *a*, *b*, or c, respectively; $U_{m,\mathrm{phase}}$ is the amplitude of the reference voltage. Overmodulation may occur if $U_{m,\mathrm{phase}}$ is large enough. The maximum value of $U_{m,\mathrm{phase}}$ not leading to overmodulation depends on not only the dc voltages but also the zero-sequence voltage as well.

Carnielutti *et al.* [22] have derived the constraint on $u_0$ to avoid overmodulation. According to [22], $u_0$ should meet the following inequation to ensure $u^*_{kg} \in [-1, 1]$:

$$u_{\min}(t) \le u_0(t) \le u_{\max}(t) \tag{2}$$

where

$$\begin{aligned} u_{\min}(t) &= \max_{k=a,b,c}(c'_k), c'_k \\ &= -U_{\mathrm{dc}k} - u_{kn}(t), k \in \{a, b, c\} \end{aligned} \tag{3}$$

$$\begin{aligned} u_{\max}(t) &= \min_{k=a,b,c}(c_k), c_k \\ &= U_{\mathrm{dc}k} - u_{kn}(t), k \in \{a, b, c\}. \end{aligned} \tag{4}$$

Note that whether (2) is valid depends on not only $u_0$ but also $u_{kn}$ and $U_{\mathrm{dc}k}$. If $u_{\min} > u_{\max}$, no matter how $u_0$ is generated, (2) cannot be satisfied and overmodulation will inevitably occur. Therefore, we should first ensure that $u_{\min} \le u_{\max}$ to avoid overmodulation. That means the following inequation must be valid:

$$-U_{\mathrm{dc}i} - u_{\mathrm{in}}(t) \le U_{\mathrm{dc}j} - u_{jn}(t), \text{ for } \forall i, j \in \{a, b, c\}. \tag{5}$$

Equation (5) can also be expressed as

$$u_{ji} \le U_{\mathrm{dc}i} + U_{\mathrm{dc}j}, \text{ for } \forall i, j \in \{a, b, c\} \tag{6}$$

where $u_{ji} = u_{jn} - u_{in}$. Considering the symmetry of the waveforms of $u_{ji}$, (6) is equivalent to

$$\begin{cases} -U_{\mathrm{dc}a} - U_{\mathrm{dc}b} \le u_{ab} \le U_{\mathrm{dc}a} + U_{\mathrm{dc}b} \\ -U_{\mathrm{dc}b} - U_{\mathrm{dcc}} \le u_{bc} \le U_{\mathrm{dc}b} + U_{\mathrm{dcc}} \\ -U_{\mathrm{dcc}} - U_{\mathrm{dc}a} \le u_{ca} \le U_{\mathrm{dcc}} + U_{\mathrm{dc}a}. \end{cases} \tag{7}$$

Considering that the line-to-line voltages must be balanced, the following inequation is valid for $\forall i, j \in$ {a, b, c}:

$$-(U_{\mathrm{dc,min}} + U_{\mathrm{dc,mid}}) \le u_{ij} \le U_{\mathrm{dc,min}} + U_{\mathrm{dc,mid}} \tag{8}$$

where $U_{\mathrm{dc,min}}$, $U_{\mathrm{dc,mid}}$, and $U_{\mathrm{dc,max}}$ are the maximum, the median, and the minimum among $U_{\mathrm{dc}a}, U_{\mathrm{dc}b}$, and $U_{\mathrm{dcc}}$, respectively. Thus, we have

$$U_{m,\mathrm{phase}} = U_{m,l-l}/\sqrt{3} \le (U_{\mathrm{dc,min}} + U_{\mathrm{dc,mid}})/\sqrt{3} \tag{9}$$

where $U_{m,l-l}$ is the amplitude of the line-to-line voltages. On the other hand, if (9) is right, (5)–(8) can be derived sequentially. Then, we can further obtain $u_{\min} \le u_{\max}$. Thus, we have

$$U_{m,\mathrm{phase}} \le (U_{\mathrm{dc,min}} + U_{\mathrm{dc,mid}})/\sqrt{3} \Leftrightarrow u_{\min} \le u_{\max}. \tag{10}$$

It can be concluded that: first, to avoid overmodulation, we should ensure that (9) is valid and that $u_0$ satisfies (2); second, the maximum amplitude of the load phase voltages achieved by linear modulation is

$$U_{\mathrm{MAX}} = (U_{\mathrm{dc,min}} + U_{\mathrm{dc,mid}})/\sqrt{3}. \tag{11}$$

As long as $u_0$ is constrained within $[u_{\min}, u_{\max}]$, overmodulation can be avoided for $\forall U_{m,\mathrm{phase}} \in [0, U_{\mathrm{MAX}}]$, and, thus, the maximum available output voltage can be achieved. According to this principle, Carnielutti *et al.* [22] gives a very simple formula for calculating $u_0$

$$u_0 = (u_{\max} + u_{\min})/2. \tag{12}$$

For $\forall U_{m,\mathrm{phase}} \in [0, U_{\mathrm{MAX}}]$, $u_0$ calculated from (12) obviously satisfies (2). Among the conventional methods based on injecting zero-sequence voltages mentioned in Section I, only the method in [22] can raise $U_{m,\mathrm{phase}}$ to $U_{\mathrm{MAX}}$ through linear modulation under all fault conditions, even when all cells in one phase are bypassed. The method in [21] can also do this in all cases except when all the cells in one phase are bypassed. The other methods can match the two methods only under some of the possible fault conditions, but in other cases they cannot always constrain $u_0$ within $[u_{\min}, u_{\max}]$, for $\forall U_{m,\mathrm{phase}} \in [0, U_{\mathrm{MAX}}]$.

The method of calculating $u_0$ is not unique. The impacts of $u_0$ on the distribution of real power should also be considered.

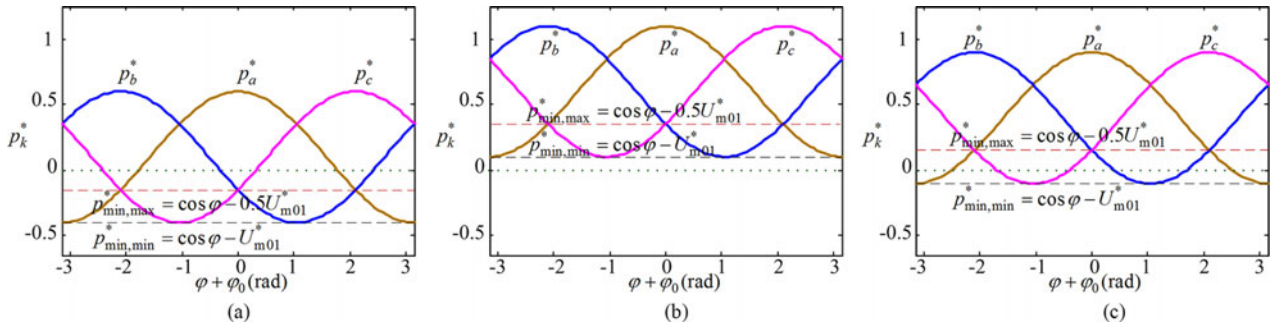


Fig. 3. Relationship curves between $p_k^*$ and $\varphi_0+\varphi$. (a) $U_{m01}^* > 2\cos\varphi$. (b) $U_{m01}^* < \cos\varphi$. (c) $2cos\varphi > U_{m01}^* > \cos\varphi$.

### *B. Requirement for the Zero-Sequence Voltage to Suppress BFRP*

Most of the loads drove by CHB inverters are approximately linear and balanced. Thus, in this paper, we assume that the inverter drives a three-phase linear and balanced load. Generally, the load currents are approximately sinusoidal. Therefore, the output current in phase *k* is assumed to be

$$i_k = I_m \sin(\omega t + \varphi_k - \varphi), k \in \{a, b, c\} \tag{13}$$

where $\varphi$ is the load PF angle and $I_m$ is the amplitude of the load current. Suppose that the fundamental component of the zero-sequence voltage is

$$u_{01} = U_{m01} \sin(\omega t + \varphi_0) \tag{14}$$

where $U_{m01}$ and $\varphi_0$ are the amplitude and the initial phase angle, respectively. Then, the fundamental component of the inverter phase voltage is expressed as follows:

$$\begin{aligned} u_{kg1} = \; & U_{m,\text{phase}} \sin(\omega t + \varphi_k) \\ & + U_{\text{m01}} \sin(\omega t + \varphi_0), k \in \{a, b, c\}. \end{aligned} \tag{15}$$

According to the definition of average power, the average power in phase *k* can be calculated from

$$\begin{aligned} p_k = \; & \left( \int_0^{2\pi} u_{kg1} i_k d\omega t \right) / (2\pi) = U_{m,\text{phase}} I_m \cos(\varphi) \\ & + U_{m01} I_m \cos(\varphi + \varphi_0 - \varphi_k). \end{aligned} \tag{16}$$

We define the normalized zero-sequence fundamental amplitude as

$$U_{m01}^* = U_{m01} / U_{m,\text{phase}} \tag{17}$$

and define the normalized average power in phase *k* as

$$\begin{aligned} p_k^*(U_{m01}^*, \varphi, \varphi_0) = \; & p_k / (U_{m,\text{phase}} I_m) = \cos(\varphi) \\ & + U_{m01}^* \cos(\varphi + \varphi_0 - \varphi_k). \end{aligned} \tag{18}$$

To avoid BFRP, we require that the real power in all three phases should be positive. That means

$$p_{\min}^* = \min_{k \in \{a,b,c\}} (p_k^*) \geq 0. \tag{19}$$

If $U_{m01}^*$ and $\varphi$ are constants, $p_k^*$ can be viewed as a function of $\varphi_0+\varphi$. Fig. 3 shows the relationship between $p_k^*$ and $\varphi_0+\varphi$ in the cases when $U_{m01}^* > 2\cos\varphi, U_{m01}^* < \cos\varphi$, and $2\cos\varphi \geq U_{m01}^* \geq \cos\varphi$.

According to (18), (19) and Fig. 3, it can be found that $p_{\min}^*$ curve is the lower envelope line of $p_a^*, p_b^*$, and $p_c^*$ curves. When $U_{m01}^* > 2\cos\varphi, p_{\min}^*$ is always negative and BFRP will inevitably occur. When $U_{m01}^* < \cos\varphi, p_{\min}^*$ is always positive and BFRP will never occur. When $2\cos\varphi \geq U_{m01}^* \geq \cos\varphi$, following inequation can be derived from $p_{\min}^* \geq 0$:

$$\begin{aligned} & (2N-1)\pi/3 + \arccos(\cos\varphi / U_{m01}^*) - \varphi_0 \leq \varphi \\ & \leq (2N+1)\pi/3 - \arccos(\cos\varphi / U_{m01}^*) - \varphi_0, N \in \mathbb{Z}. \end{aligned} \tag{20}$$

According to the above analysis, the following conclusions can be drawn.

First, either of the following two conditions must be satisfied to avoid BFRP: first, $U_{m01}^* < \cos\varphi$; second, $2\cos\varphi \geq U_{m,01}^* \geq \cos\varphi$ and (20) is valid.

Second, if $\varphi$ and $\varphi_0$ are constants, the real power is more likely to flow back as $U_{m01}^*$ becomes larger. Suppose that ∃A, B∈[0, 1] and A > B. If $p_{min}^* < 0$ when $U_{m01}^* = A$, we also have $p_{min}^* < 0$ when $U_{m01}^* = B$.

Third, if $U_{m01}^*$ and $\varphi$ are constants, $p_{\min}^*$ is a periodical function of $\varphi_0$, and the period is $2\pi/3$.

### *C. Definition of the Conservative Range of the PF Angle (CRPA)*

The first conclusion above implies that it is impossible to avoid BFRP, for $\forall\varphi \in [-\pi/2, \pi/2]$ as long as $u_0$ has a fundamental component. However, $u_0$ must be limited within $[u_{\min}, u_{\max}]$ to avoid overmodulation. In Section III, it will be seen that the region between the waveforms of $u_{\min}$ and $u_{\max}$ under fault conditions may be so unregular that the fundamental component of $u_0$ is difficult to eliminate completely. Therefore, the range of $\varphi$ that the inverter can tolerate without degrading output voltage capability or inducing BFRP cannot be easily extended to $[-\pi/2, \pi/2]$. Nevertheless, the range is expected to be as wide as possible. The wider the range, the lower the possibility of BFRP is. Thus, the range can be used to evaluate the ability of a method based on zero-sequence voltage injection to suppress BFRP. Considering that this range is also affected by $U_{\text{dc}k}$ and $U_{m,\text{phase}}$, the range is expressed mathematically by the concept of CRPA defined as follows.

Suppose that a certain method based on zero-sequence voltage injection is used. Given a set of $(U_{\text{dc}a}, U_{\text{dc}b}, U_{\text{dc}c})$, if $[\varphi_{\min}, \varphi_{\max}]$ meets both of the following conditions: first, for $\forall\varphi \in [\varphi_{\min}, \varphi_{\max}]$ and $\forall U_{m,\text{phase}} \in [0, U_{\text{MAX}}]$, $p_{\min}^* \geq$

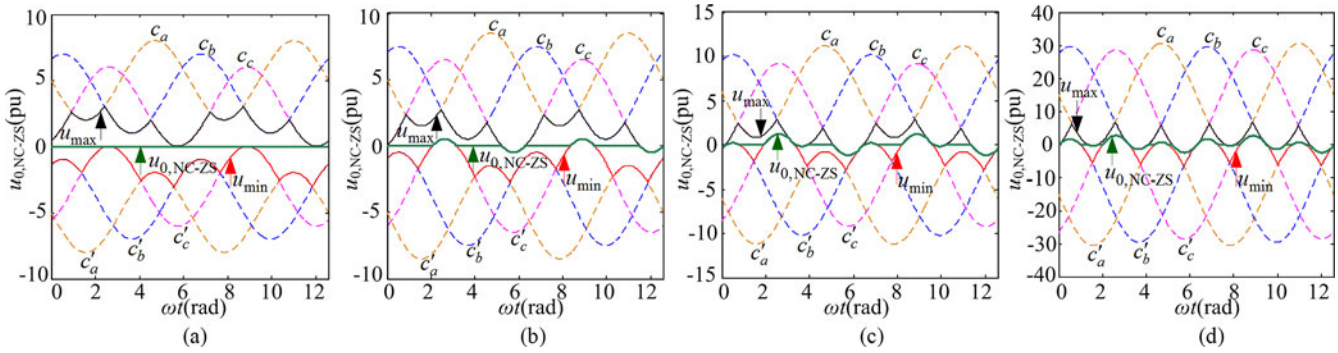


Fig. 4. NC-ZS signals. (a) 0-type. (b) I-type. (c) II-type. (d) III-type.

0; second, for $\forall\varphi\in[-\pi/2,\varphi_{\min})\cup(\varphi_{\max},\pi/2]$, $\exists U_{m,\text{phase}}\in[0,U_{\text{MAX}}]$ such that $p^*_{\min}<0$, then the interval $[\varphi_{\min},\varphi_{\max}]$ is referred to as the CRPA of the method under the condition of $(U_{\text{dca}},U_{\text{dcb}},U_{\text{dcc}})$.

This concept is defined only for those methods that can raise $U_{m,\text{phase}}$ to $U_{\text{MAX}}$, such as the methods proposed in [21] and [22]. As for the methods that cannot raise $U_{m,\text{phase}}$ to $U_{\text{MAX}}$, their CRPA will be not discussed in this paper, since those methods have a disadvantage in terms of output voltage capability.

## III. Generation of the Zero-Sequence Voltage

To make the CRPA as wide as possible, we should first ensure that $u_0$ is always constrained within $[u_{\min},u_{\max}]$, for $\forall U_{m,\text{phase}}\in[0,U_{\text{MAX}}]$. Then, according to the second conclusion mentioned in Section II-B, the smaller $U^*_{m01}$, the less likely the real power is to flow back. Therefore, the possibility of BFRP can be effectively reduced if $U^*_{m01}$ is made as small as possible.

The process of confining $u_0$ within $[u_{\min},u_{\max}]$ can be achieved by a saturation link, the lower and upper limits of which are $u_{\min}$ and $u_{\max}$, respectively. The output of the link can be used as $u_0$. Now, the problem is how to find an appropriate input signal to make the fundamental component of the output as small as possible. It is a challenge because the limits of the saturation link are dynamic and unregular.

In this section, the problem is solved step by step. First, we temporarily set the input signal of the saturation link to 0. The output signal obtained can be viewed as an embryonic form of $u_0$. The output signal is called a naturally clipped zero-sequence (NC-ZS) signal, which is denoted by $u_{0,\text{NC-ZS}}$. Then, the saturation limits are regularized. Finally, we select a more appropriate signal as the input so that the fundamental component in the output can be effectively reduced.

### A. NC-ZS Signals

There are four types of NC-ZS signals.

*0-type:* When $U_{m,\text{phase}}\le U_{\text{dc,min}}$, $u_{0,\text{SC-ZS}}\equiv 0$. Fig. 4(a) shows an example, in which $(U_{\text{dca}},U_{\text{dcb}},U_{\text{dcc}})=(5,4,3)$ and $U_{m,\text{phase}}=3$.

*I-type:* When $U_{\text{dc,min}}<U_{m,\text{phase}}\le U_{\text{dc,mid}}$, the zero signal is clipped only once per half cycle of reference voltages on average. Fig. 4(b) shows an example, in which $(U_{\text{dca}},U_{\text{dcb}},U_{\text{dcc}})=(5,4,3)$ and $U_{m,\text{phase}}=3.5$.

*II-type:* When $U_{\text{dc,mid}}<U_{m,\text{phase}}\le\min(U_{\text{MAX}},U_{\text{dc,max}})$, the zero signal is clipped twice per half cycle of reference voltages on average. Fig. 4(c) shows an example, in which $(U_{\text{dca}},U_{\text{dcb}},U_{\text{dcc}})=(6,5,4)$, $U_{m,\text{phase}}=5.196$.

*III-type:* When $U_{\text{dc,max}}<U_{m,\text{phase}}\le U_{\text{MAX}}$, the zero signal is clipped three times per half cycle of reference voltages on average. Fig. 4(d) shows an example, in which $(U_{\text{dca}},U_{\text{dcb}},U_{\text{dcc}})=(15,14,13)$, $U_{m,\text{phase}}=15.588$.

Obviously, apart from 0-type NC-ZS signals, the other three types of NC-ZS signals inevitably have fundamental components. It can be found that the waveform of $u_{0,\text{NC-ZS}}$ can be reshaped within the region between the waveforms of $u_{\min}$ and $u_{\max}$ so that its fundamental component can be further reduced. Nevertheless, the irregularity of the waveforms of $u_{\min}$ and $u_{\max}$ makes it difficult to reshape $u_{0,\text{NC-ZS}}$. Therefore, it is necessary to regularize the waveforms of $u_{\min}$ and $u_{\max}$. Furthermore, the revision of $u_{\min}$ and $u_{\max}$ must follow two principles: not degrading the available output voltage and not increasing the fundamental component in the output of the saturation link.

### B. Revision of the Saturation Limits and Symmetrically Clipped Zero-Sequence (SC-ZS) Signals

According to (11), $U_{\text{MAX}}$ is affected only by $U_{\text{dc,min}}$ and $U_{\text{dc,mid}}$. Therefore, if we replace $U_{\text{dc,max}}$ with $U_{\text{dc,mid}}$ when calculating $u_{\min}$ and $u_{\max}$, we still have $u_{\max}\ge u_{\min}$ for $\forall U_{m,\text{phase}}\in[0,U_{\text{MAX}}]$. Thus, the maximum available output voltage will not change. The new available dc voltage in phase *k* can be defined as

$$U_{\text{dc}k,s}=\begin{cases}U_{\text{dc,mid}}, & \text{when } U_{\text{dc}k}=U_{\text{dc,max}}\\ U_{\text{dc}k}, & \text{when } U_{\text{dc}k}\ne U_{\text{dc,max}}.\end{cases}\tag{21}$$

Replacing $U_{\text{dc}k}$ in (3), (4) with $U_{\text{dc}k,s}$ leads to new $c_k$, $c'_k$, $u_{\min}$, and $u_{\max}$, which are denoted by $c_{k,s}$, $c'_{k,s}$, $u_{\min,s}$, and $u_{\max,s}$, respectively. If the input of the saturation link is still 0, the new output signal is referred to as an SC-ZS signal, which is denoted by $u_{0,\text{SC-ZS}}$. There are only three types of SC-ZS signals.

*0-type:* When $U_{m,\text{phase}}\le U_{\text{dc,min}}$, $u_{0,\text{SC-ZS}}\equiv 0$. Fig. 5(a) shows an example, where $U_{\text{dc}k}$ and $U_{m,\text{phase}}$ are the same as those in Fig. 4(a).

*I-type:* When $U_{\text{dc,min}}<U_{m,\text{phase}}\le U_{\text{dc,mid}}$, the zero signal is clipped only once per half cycle of the reference voltages on

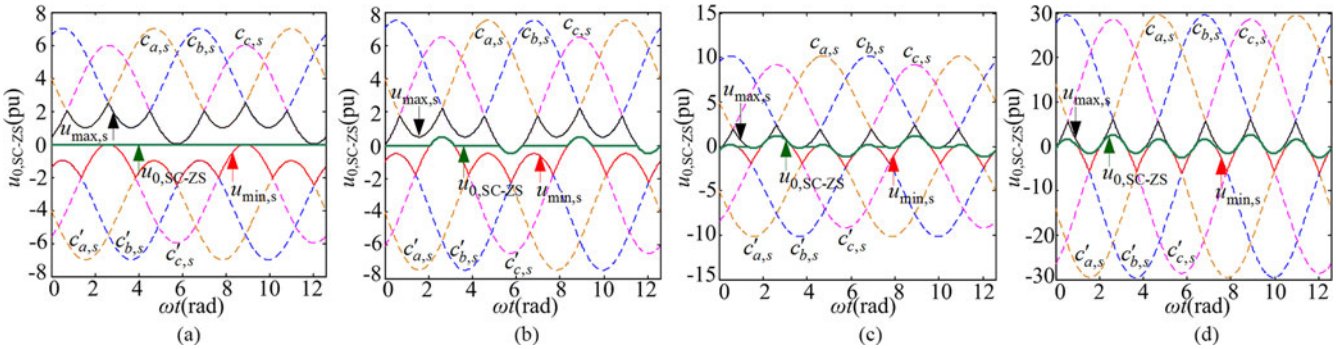


Fig. 5. SC-ZS signals. (a) 0-type. (b) I-type. (c) III-type, $(U_{\mathrm{dc}a}, U_{\mathrm{dc}b}, U_{\mathrm{dc}c}) = (6, 5, 4)$, $U_{m,\mathrm{phase}} = 5.196$. (d) III-type, $(U_{\mathrm{dc}a}, U_{\mathrm{dc}b}, U_{\mathrm{dc}c}) = (15, 14, 13)$, $U_{m,\mathrm{phase}} = 15.588$.

average. Fig. 5(b) shows an example, where $U_{\mathrm{dc}k}$ and $U_{m,\mathrm{phase}}$ are the same as those in Fig. 4(b).

*III-type:* When $U_{\mathrm{dc,mid}} < U_{m,\mathrm{phase}} \le U_{\mathrm{MAX}}$, the zero signal is clipped three times per half cycle of the reference voltages on average. Fig. 5(c) shows an example, where $U_{\mathrm{dc}k}$ and $U_{m,\mathrm{phase}}$ are the same as those in Fig. 4(c); Fig. 5(d) shows another example, where $U_{\mathrm{dc}k}$ and $U_{m,\mathrm{phase}}$ are the same as those in Fig. 4(d).

It can be seen from Fig. 5 that the waveforms of $u_{\min}$ and $u_{\max}$ both have reflection symmetry, which will help to further reshape the waveform of SC-ZS signals.

As mentioned at the end of Section II-A, the revision of $u_{\min}$ and $u_{\max}$ should not increase the fundamental component in the output of the saturation link. After the revision, NC-ZS signals are changed into SC-ZS signals. Based on Fourier analysis, their fundamental amplitudes can be compared. Although there are different types of NC-ZS signals and SC-ZS signals, they can be written in a uniform way

$$u_{0,\mathrm{NC-ZS}} = u_{\mathrm{I}a} + u_{\mathrm{I}b} + u_{\mathrm{I}c} \tag{22}$$

$$u_{0,\mathrm{SC-ZS}} = u_{\mathrm{I}a,s} + u_{\mathrm{I}b,s} + u_{\mathrm{I}c,s} \tag{23}$$

where

$$u_{\mathrm{I}k} = \begin{cases} c_k, & \text{when } c_k < 0 \\ 0, & \text{when } c'_k < 0 < c_k \\ c'_k, & \text{when } c'_k > 0 \end{cases}, k \in \{a, b, c\} \tag{24}$$

$$u_{\mathrm{I}k,s} = \begin{cases} c_{k,s}, & \text{when } c_{k,s} < 0 \\ 0, & \text{when } c'_{k,s} < 0 < c_{k,s} \\ c'_{k,s}, & \text{when } c'_{k,s} > 0 \end{cases}, k \in \{a, b, c\}. \tag{25}$$

We call $u_{\mathrm{I}k}$ the I-type component of an NC-ZS signal and call $u_{\mathrm{I}k,s}$ the I-type component of an SC-ZS signal. Fig. 6 shows a typical waveform of $u_{\mathrm{I}k}$ or $u_{\mathrm{I}k,s}$ in one period. From Fourier decomposition, the fundamental component of $u_{\mathrm{I}k}$ can be derived, which is

$$u_{\mathrm{I}k1}(t) = U_{\mathrm{Im}}(U_{\mathrm{dc}k})\sin(\omega t + \varphi_k + \pi), k \in \{a, b, c\} \tag{26}$$

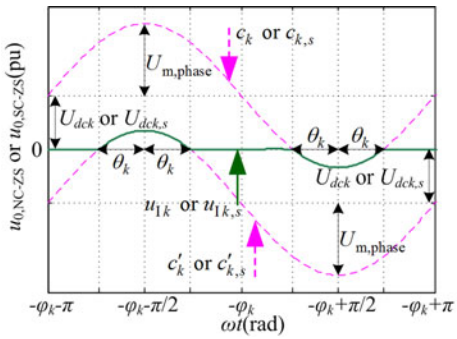


Fig. 6. Typical waveform of I-type component of an NC-ZS or SC-ZS signal in one period.

where $U_{\mathrm{Im}}$ is a function of $U_{\mathrm{dc}k}$

$$U_{\mathrm{Im}}(U_{\mathrm{dc}k}) = U_{m,\mathrm{phase}}[2\theta_k(U_{\mathrm{dc}k}) - \sin(2\theta_k(U_{\mathrm{dc}k}))]/\pi \tag{27}$$

$$\theta_k(U_{\mathrm{dc}k}) = \begin{cases} \arccos(U_{\mathrm{dc}k}/U_{m,\mathrm{phase}}), & U_{\mathrm{dc}k} < U_{m,\mathrm{phase}} \\ 0, & U_{\mathrm{dc}k} \ge U_{m,\mathrm{phase}}. \end{cases} \tag{28}$$

Replacing the $U_{\mathrm{dc}k}$ with $U_{\mathrm{dc}k,s}$ in (27), (28), we obtain the fundamental component of $u_{\mathrm{I}k,s}$

$$u_{\mathrm{I}k1,s}(t) = U_{\mathrm{Im}}(U_{\mathrm{dc}k,s})\sin(\omega t + \varphi_k + \pi), k \in \{a, b, c\}. \tag{29}$$

Suppose that the fundamental components of $u_{0,\mathrm{NC-ZS}}$ and $u_{0,\mathrm{SC-ZS}}$ are $u_{01,\mathrm{NC-ZS}}$ and $u_{01,\mathrm{SC-ZS}}$, respectively. Obviously, we have $u_{01,\mathrm{NC-ZS}} = u_{\mathrm{I}a1} + u_{\mathrm{I}b1} + u_{\mathrm{I}c1}$ and $u_{01,\mathrm{SC-ZS}} = u_{\mathrm{I}a1,s} + u_{\mathrm{I}b1,s} + u_{\mathrm{I}c1,s}$. Without loss of generality, we assume that $U_{\mathrm{dc}a} = U_{\mathrm{dc,max}}, U_{\mathrm{dc}b} = U_{\mathrm{dc,mid}}$, and $U_{\mathrm{dc}c} = U_{\mathrm{dc,min}}$. In this paper, if $x = X_{\mathrm{m}}\sin(\omega t + \varphi_x)$, the phasor of $x$ is expressed as $\mathbf{X} = X_{\mathrm{m}}\varphi_x$. Thus, we have $\mathbf{U}_{\mathrm{I}a1} = U_{\mathrm{Im}}(U_{\mathrm{dc,max}})\pi$ ; $\mathbf{U}_{\mathrm{I}b1} = U_{\mathrm{Im}}(U_{\mathrm{dc,mid}}) \angle \pi/3$; $\mathbf{U}_{\mathrm{I}c1} = U_{\mathrm{Im}}(U_{\mathrm{dc,min}}) \angle 5\pi/3$; $\mathbf{U}_{\mathrm{I}a1,s} = U_{\mathrm{Im}}(U_{\mathrm{dc,mid}}) \angle \pi$ ; $\mathbf{U}_{\mathrm{I}b1,s} = U_{\mathrm{Im}}(U_{\mathrm{dc,mid}})\pi/3$; and $\mathbf{U}_{\mathrm{I}c1,s} = U_{\mathrm{Im}}(U_{\mathrm{dc,mid}}) \angle 5\pi/3$. Then, the phasors of $u_{01,\mathrm{NC-ZS}}$ and $u_{01,\mathrm{SC-ZS}}$ can be calculated from

$$\boldsymbol{U}_{01,\mathrm{NC-ZS}} = \boldsymbol{U}_{Ia1} + \boldsymbol{U}_{Ib1} + \boldsymbol{U}_{Ic1} = U_{m01,\mathrm{NC-ZS}} \angle \varphi_{\mathrm{NC-ZS}} \tag{30}$$

$$\begin{aligned} \boldsymbol{U}_{01,\mathrm{SC-ZS}} &= \boldsymbol{U}_{Ia1,s} + \boldsymbol{U}_{Ib1,s} + \boldsymbol{U}_{Ic1,s} \\ &= U_{m01,\mathrm{SC-ZS}} \angle \varphi_{\mathrm{SC-ZS}} \end{aligned} \tag{31}$$

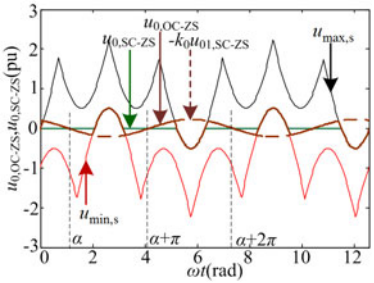


Fig. 7. Waveform of an OC-ZS signal.

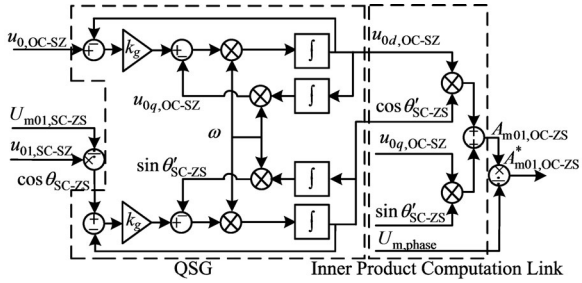


Fig. 8. Detection of $A^*_{m\,01,\mathrm{OC-ZS}}$.

where

$$U_{m01,\mathrm{NC-ZS}} = \{[U_{\mathrm{Im}}(U_{\mathrm{dc,max}}) - U_{\mathrm{Im}}(U_{\mathrm{dc,mid}})/2 - U_{\mathrm{Im}}(U_{\mathrm{dc,min}})/2]^2 + 0.75[U_{\mathrm{Im}}(U_{\mathrm{dc,mid}}) - U_{\mathrm{Im}}(U_{\mathrm{dc,min}})]^2\}^{1/2} \quad (32)$$

$$\varphi_{\mathrm{NC-ZS}} = \arctan\left[\left(\sqrt{3}U_{\mathrm{Im}}(U_{\mathrm{dc,mid}}) - \sqrt{3}U_{\mathrm{Im}}(U_{\mathrm{dc,min}})\right) / (U_{\mathrm{Im}}(U_{\mathrm{dc,mid}}) + U_{\mathrm{Im}}(U_{\mathrm{dc,min}}) - 2U_{\mathrm{Im}}(U_{\mathrm{dc,max}}))\right] + 2N\pi \quad (33)$$

$$U_{m01,\mathrm{SC-ZS}} = U_{\mathrm{Im}}(U_{\mathrm{dc,min}}) - U_{\mathrm{Im}}(U_{\mathrm{dc,mid}}) \quad (34)$$

$$\varphi_{\mathrm{SC-ZS}} = \varphi_c + \pi + 2N\pi, N \in \mathbb{Z}. \quad (35)$$

Because the derivative of $U_{\mathrm{Im}}$ with respect to $U_{dck}$ is always nonpositive, we have $U_{\mathrm{Im}}(U_{\mathrm{dc,max}}) \le U_{\mathrm{Im}}(U_{\mathrm{dc,mid}}) \le U_{\mathrm{Im}}(U_{\mathrm{dc,min}})$. As a result

$$U^2_{m01,\mathrm{NC-ZS}} - U^2_{m01,\mathrm{SC-ZS}} = [U_{\mathrm{Im}}(U_{\mathrm{dc,max}}) - U_{\mathrm{Im}}(U_{\mathrm{dc,mid}})] \cdot [U_{\mathrm{Im}}(U_{dc,\mathrm{max}}) - U_{\mathrm{Im}}(U_{\mathrm{dc,min}})] \ge 0. \quad (36)$$

Therefore, the fundamental amplitude of $u_{0,\mathrm{SC-ZS}}$ is not larger than that of $u_{0,\mathrm{NC-ZS}}$. The revision of $u_{\min}$ and $u_{\max}$ does not increase the fundamental component in the output signal of the saturation link.

Moreover, if $u_{xn,\mathrm{dcmin}}$ denotes the reference voltage in the phase with the smallest available dc voltage, it can be seen from (35) that the phase difference between $u_{01,\mathrm{SC-ZS}}$ and $u_{xn,\mathrm{dcmin}}$ is $\pi$. Therefore, $u_{01,\mathrm{SC-ZS}}$ can be expressed as

$$u_{01,\mathrm{SC-ZS}} = -U_{m01,\mathrm{SC-ZS}}u_{xn,\mathrm{dcmin}}/U_{m,\mathrm{phase}}. \quad (37)$$

### C. Oppositely Clipped Zero-Sequence (OC-ZS) Control Method

Now, the waveforms of the saturation limits have reflection symmetry, which makes it easy to select a more appropriate signal as the input signal of the saturation link. Obviously, the signal $-k_0u_{01,\mathrm{SC-ZS}}$ is a good choice. Here, $k_0$ is a nonnegative coefficient. If $-k_0u_{01,\mathrm{SC-ZS}}$ instead of zero is used as the input signal of the saturation link, a new output signal can be obtained. It is referred to as an OC-ZS signal and denoted by $u_{0,\mathrm{OC-ZS}}$. Its fundamental component is denoted by $u_{01,\mathrm{OC-ZS}}$. Fig. 7 shows the waveform of $u_{0,\mathrm{OC-ZS}}$. When $k_0 = 0$, we obviously have $u_{0,\mathrm{OC-ZS}} = u_{0,\mathrm{SC-ZS}}$ and $u_{01,\mathrm{OC-ZS}} = u_{01,\mathrm{SC-ZS}}$. With $k_0$ increasing from 0, the waveform of $u_{0,\mathrm{OC-ZS}}$ will have negative parts over the interval $[\alpha, \alpha+\pi]$ and positive parts over the interval $[\alpha+\pi, \alpha+2\pi]$, as shown in Fig. 7. According to the Fourier analysis and the symmetry of the waveform of $u_{0,\mathrm{OC-ZS}}$, the amplitude of $u_{01,\mathrm{OC-ZS}}$ will drop from the amplitude of $u_{01,\mathrm{SC-ZS}}$ down to 0 as $k_0$ rises from 0.

In some cases, the region between the waveforms of $u_{\max,s}$ and $u_{\min,s}$ is so narrow that the amplitude of $u_{01,\mathrm{OC-ZS}}$ cannot be reduced to 0 even if $k_0$ increases to $+\infty$. In some other cases, the region is wide enough so that the amplitude of $u_{01,\mathrm{OC-ZS}}$ is reduced to 0 when $k_0$ reaches a certain value. However, if $k_0$ continues increasing, the amplitude of $u_{01,\mathrm{OC-ZS}}$ will increase. Therefore, $k_0$ must be set to an appropriate value.

Feedback control is used to find an appropriate $k_0$ in this paper. Here, the algebraic amplitude of $u_{01,\mathrm{OC-ZS}}$ is defined as a quantity that has the same absolute value as the amplitude of $u_{01,\mathrm{OC-ZS}}$ and has the same sign as the product of $u_{01,\mathrm{OC-ZS}}$ and $u_{01,\mathrm{SC-ZS}}$. The quantity is denoted by $A_{m01,\mathrm{OC-ZS}}$. We also define the normalized value of $A_{m01,\mathrm{OC-ZS}}$ as $A^*_{m01,\mathrm{OC-ZS}} = A_{m01,\mathrm{OC-ZS}}/U_{m,\mathrm{phase}}$. The value of $k_0$ is adjusted according to the value of $A^*_{m01,\mathrm{OC-ZS}}$. When $A^*_{m01,\mathrm{OC-ZS}} > 0$, we increase $k_0$. When $A^*_{m01,\mathrm{OC-ZS}} < 0$, we reduce $k_0$. Finally, the fundamental component of $u_{0,\mathrm{OC-ZS}}$ will be as small as possible. The control method described above is referred to as OC-ZS control.

In the control process, the adjustment of $k_0$ can be implemented by a PI controller. $A^*_{m01,\mathrm{OC-ZS}}$ can be detected by the method illustrated in Fig. 8, in which there are two quadrature signal generators based on second-order general integrator [30] and one inner product computation link. According to [30], the gain $k_g$ should be 1.414 to acquire an optimal damping factor. The whole process of OC-ZS control is shown in Fig. 9.

In Fig. 9, $u_{an}, u_{bn}, u_{cn}$, $U_{m,\mathrm{phase}}$, and $\omega$ depend on other control objectives; $U_{\mathrm{dca}}, U_{\mathrm{dcb}}$, and $U_{\mathrm{dcc}}$ are determined by dc voltages of the cells and the number of normal cells in each phase. The PI controller automatically adjusts $k_0$ according to the value of $A^*_{m01,\mathrm{OC-ZS}}$. The lower output limit of the PI is set to 0 so that $k_0 \ge 0$. Thus, the amplitude of $u_{01,\mathrm{OC-ZS}}$ will be always smaller than that of $u_{01,\mathrm{SC-ZS}}$. The final output signal $u_0$, namely $u_{0,\mathrm{OC-ZS}}$ will be used in the modulation process depicted by Fig. 2.

### D. Ability of OC-ZS Control to Suppress BFRP

In Section II-C, the concept of CRPA is defined to evaluate the ability of a method based on zero-sequence voltage injection

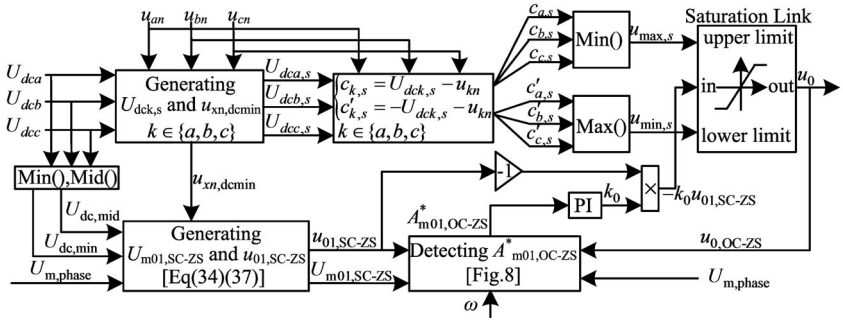


Fig. 9. Diagram of an OC-ZS control.

to suppress BFRP. The CRPA of OC-ZS control is difficult to determine exactly because it is affected by the parameters of the PI controller in Fig. 9. However, we have known that the amplitude of $u_{01,\mathrm{OC-ZS}}$ is always smaller than that of $u_{01,\mathrm{SC-ZS}}$. Thus, if the method that SC-ZS signals are used as $u_0$ is referred to as SC-ZS method, the CRPA of OC-ZS control is at least wider than that of the SC-ZS method. Therefore, the CRPA of the SC-ZS method can be viewed as a conservative evaluation of the CRPA of an OC-ZS control.

According to (18), (19), $p^*_{\min}$ is a function of $U^*_{m01}$, $\varphi$, and $\varphi_0$. When $u_0 = u_{0,\mathrm{SC-ZS}}, U^*_{m01}$ can be expressed according to (17), (34) by (38) as shown at the bottom of the page, where

$$\theta_{\min} = \arccos(U_{\mathrm{dc,min}}/U_{m,\mathrm{phase}}) \tag{39}$$

$$\theta_{\mathrm{mid}} = \arccos(U_{\mathrm{dc,mid}}/U_{m,\mathrm{phase}}). \tag{40}$$

Given a set of ($U_{\mathrm{dc}a}$, $U_{\mathrm{dc}b}$, $U_{\mathrm{dc}c}$), $U^*_{m01}$ is a function of $U_{m,\mathrm{phase}}$. The function is represented by $U^*_{m01}(U_{m,\mathrm{phase}})$. Therefore, $p^*_{\min}$ is also a function of $U_{m,\mathrm{phase}}$, $\varphi$, and $\varphi_0$, and can be expressed as $p^*_{\min} = p^*_{\min}(U^*_{m01}(U_{m,\mathrm{phase}}), \varphi, \varphi_0)$. When $u_0 = u_{0,\mathrm{SC-ZS}}$, $\varphi_0$ defined in (14) may be $\pi$ or $\pm\pi/3$ according to (37). However, according to the third conclusion in Section II-B, $p^*_{\min}$ is a periodical function of $\varphi_0$ and the period is $2\pi/3$. Thus, it makes no difference whether $\varphi_0$ equals $\pi$ or $\pm\pi/3$, so $\varphi_0$ can be set to $\pi$. Now, $p^*_{\min}$ is affected only by $U_{m,\mathrm{phase}}$ and $\varphi$. For each value of $U_{m,\mathrm{phase}}$ that belongs to [0, $U_{\mathrm{MAX}}$], we can derive a range of $\varphi$ satisfying $p^*_{\min} \geq 0$. When $u_0 = u_{0,\mathrm{SC-ZS}}$, the CRPA is the intersection of all such ranges. There are infinite values in [0, $U_{\mathrm{MAX}}$], so it is impossible to obtain all the ranges. However, according to the second conclusion in Section II-B, the real power is most likely to flow back when $U^*_{0m1}$ reaches its maximum value. Therefore, when $U^*_{0m1}$ equals its maximum value, the range of $\varphi$ satisfying $p^*_{\min} \geq 0$ is the narrowest one, namely the CRPA of the SC-ZS method.

It is easy to prove that $U^*_{m01}$ is a continuous function of $U_{m,\mathrm{phase}}$ when $U_{m,\mathrm{phase}} \in [0, U_{\mathrm{MAX}}]$ and that the function is piecewise differentiable. When $U_{\mathrm{dc,min}} < U_{m,\mathrm{phase}} < U_{\mathrm{dc,mid}}$, we have $dU^*_{m01}/d\theta_{\min} = 2(1-\cos 2\theta_{\min})/\pi > 0$. According to (39), $\theta_{\min}$ is an increasing function of $U_{m,\mathrm{phase}}$. Therefore, $U^*_{m01}$ is an increasing function of $U_{m,\mathrm{phase}}$ when $U_{\mathrm{dc,min}} < U_{m,\mathrm{phase}} < U_{\mathrm{dc,mid}}$. When $U_{m,\mathrm{phase}} > U_{\mathrm{dc,mid}}$, we have

$$\frac{dU^*_{m01}}{dU_{m,\mathrm{phase}}} = \frac{4\cos(\theta_{\min}+\theta_{\mathrm{mid}})\sin(\theta_{\min}-\theta_{\mathrm{mid}})}{\pi U_{m,\mathrm{phase}}}. \tag{41}$$

According to (39), (40), $\pi/2 > \theta_{\min} > \theta_{\mathrm{mid}} > 0$, so $\sin(\theta_{\min}-\theta_{\mathrm{mid}}) > 0$. If $\theta_{\min}+\theta_{\mathrm{mid}} = \pi/2, U_{m,\mathrm{phase}}$ equals $\sqrt{U^2_{\mathrm{mid}}+U^2_{\min}}$. It is easy to prove that the following inequation is always valid:

$$\begin{aligned}\sqrt{U^2_{\mathrm{dc,mid}}+U^2_{\mathrm{dc,min}}} &> \frac{U_{\mathrm{dc,mid}}+U_{\mathrm{dc,min}}}{\sqrt{3}} \\ &= U_{\mathrm{MAX}} \geq U_{m,\mathrm{phase}}.\end{aligned} \tag{42}$$

Furthermore, $\theta_{\min}+\theta_{\mathrm{mid}}$ is obviously an increasing function of $U_{m,\mathrm{phase}}$. As a result, we have $\theta_{\min}+\theta_{\mathrm{mid}} < \pi/2$ and $\cos(\theta_{\min}+\theta_{\mathrm{mid}}) > 0$. Thus, $dU^*_{m01}/dU_{m,\mathrm{phase}} > 0$ and $U^*_{m01}$ is still an increasing function of $U_{m,\mathrm{phase}}$ when $U_{m,\mathrm{phase}} \in (U_{\mathrm{dc,mid}}, U_{\mathrm{MAX}}]$. According to the above analysis, $U^*_{m01}$ is an increasing function of $U_{m,\mathrm{phase}}$ when $U_{m,\mathrm{phase}} \in [0, U_{\mathrm{MAX}}]$, so the maximum of $U^*_{m01}$ is $U^*_{m01}(U_{\mathrm{MAX}})$. The boundary values of the CRPA, namely $\varphi_{\min}$ and $\varphi_{\max}$, are the solutions for $\varphi$ in the following equation:

$$p^*_{\min} = \min_{k=a,b,c}\left(p^*_k\left(U^*_{m01}(U_{\mathrm{MAX}}), \varphi, \pi\right)\right) = 0, \varphi \in \left[-\frac{\pi}{2}, \frac{\pi}{2}\right]. \tag{43}$$

This is a nonlinear equation which can be solved by numerical methods. For example, suppose that every phase has five cells and $V_{\mathrm{dc,cell}}$ is 1; $N_{\max}, N_{\mathrm{mid}}$, and $N_{\min}$ denote the maximum, the median, and the minimum among $N_a, N_b$, and $N_c$, respectively; $N_{\max} = x \geq 4, N_{\mathrm{mid}} = 4$ and $N_{\min} = 1$. In this case, $(U_{\mathrm{dc,max}}, U_{\mathrm{dc,mid}}, U_{\mathrm{dc,min}}) = (x, 4, 1)$. Thus, $U_{\mathrm{MAX}}$ equals 2.8868. On substituting this value into (43) and solving for $\varphi$ by fsolve function in MATLAB, we have $\varphi = \pm 1.2050$,

$$U^*_{m01} = U_{m01,\mathrm{SC-ZS}}/U_{m,\mathrm{phase}} = \begin{cases} 0, & U_{m,\mathrm{phase}} \leq U_{\mathrm{dc,min}} \\ (2\theta_{\min} - \sin 2\theta_{\min})/\pi, & U_{\mathrm{dc,min}} < U_{m,\mathrm{phase}} \leq U_{\mathrm{dc,mid}} \\ \dfrac{(2\theta_{\min} - \sin 2\theta_{\min}) - (2\theta_{\mathrm{mid}} - \sin 2\theta_{\mathrm{mid}})}{\pi}, & U_{\mathrm{dc,mid}} < U_{m,\mathrm{phase}} \end{cases} \tag{38}$$

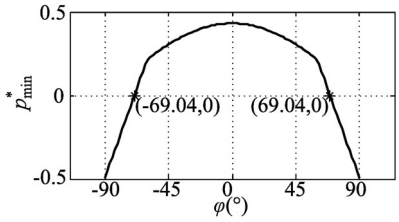


Fig. 10. $p^*_{\min} - \varphi$ curve when $(U_{\mathrm{dc,max}}, U_{\mathrm{dc,mid}}, U_{\mathrm{dc,min}}) = (x, 4, 1)$.

TABLE I
CRPA AND THE MAXIMUM AMPLITUDES OF THE LINE-TO-LINE VOLTAGES WHEN SC-ZS METHOD IS USED

| $(N_{\max}, N_{\mathrm{mid}}, N_{\min})$ | $[\varphi_{\min}, \varphi_{\max}]/°$ | $U_{l-l,\max}/\mathrm{p.u.}$ |
|---|---|---|
| (5, 5, 5) | [−90, 90] | 10 |
| (5, 5, 4) | [−84.43, 84.43] | 9 |
| (5, 5, 3) | [−79.65, 79.65] | 8 |
| (5, 5, 2) | [−74, 74] | 7 |
| (5, 5, 1) | [−67, 67] | 6 |
| (5, 5, 0) | [−60, 60] | 5 |
| (*x*, 4, 4) | [−90, 90] | 8 |
| (*x*, 4, 3) | [−83.13, 83.13] | 7 |
| (*x*, 4, 2) | [−76.98, 76.98] | 6 |
| (*x*, 4, 1) | [−69.04, 69.04] | 5 |
| (*x*, 4, 0) | [−60, 60] | 4 |
| (*x*, 3, 3) | [−90, 90] | 6 |
| (*x*, 3, 2) | [−81.27, 81.27] | 5 |
| (*x*, 3, 1) | [−71.86, 71.86] | 4 |
| (*x*, 3, 0) | [−60, 60] | 3 |
| (*x*, 2, 2) | [−90, 90] | 4 |
| (*x*, 2, 1) | [−76.98, 76.98] | 3 |
| (*x*, 2, 0) | [−60, 60] | 2 |
| (*x*, 1, 1) | [−90, 90] | 2 |
| (*x*, 1, 0) | [−60, 60] | 1 |

namely ±69.04°. Therefore, the CPRA in this case is [−69.04°, 69.04°], and the $p^*_{\min} - \varphi$ curve is plotted, as shown in Fig. 10.

Similar methods can be used to obtain the CRPA of SC-ZS method under any set of $(N_{\max}, N_{\mathrm{mid}}, N_{\min})$. Table I lists the results as well as the maximum achievable amplitudes of the line-to-line voltages, which can be calculated from (9).

If $U_{m,\mathrm{phase}}$ is set to $U_{\mathrm{MAX}}$ and $\varphi$ is set to $\varphi_{\min}$ or $\varphi_{\max}$ listed in Table I, it can be verified through simulations or experiments that the method in [22] will lead to BFRP in all fault conditions except when $N_{\min} = 0$. When $N_{\min} = 0$, according to (3), (4), we have $u_{\max} = u_{\min} = -u_{xn,\mathrm{dcmin}}$. Thus, $u_0$ can only be $-u_{xn,\mathrm{dcmin}}$. As a result, the CRPA of either the method in [22] or SC-ZS method is [−60°, 60°]. Therefore, the CRPA of the method in [22] is narrower than that of the SC-ZS method when $N_{\min} \neq 0$ and is the same as that of the SC-ZS method when $N_{\min} = 0$. This means that the SC-ZS method is preferable to the method in [22] in terms of suppressing BFRP. Therefore, OC-ZS control is also better than the method in [22] in terms of suppressing BFRP.

## IV. EXPERIMENTAL RESULTS

The experimental circuit was similar to the circuit in Fig. 1, but the difference was that there were no bypass contactors in the experimental circuit. A cell could be bypassed by keeping its two upper IGBTs on and its two lower IGBTs off. The experimental platform is shown in Fig. 11. The whole inverter was controlled by a main controller, which was responsible for calculating the normalized modulating signals ($u^*_{kg}$) and transferring these signals to 15 cell controllers. The cell controllers sampled the received signals at a rate of 5000 Hz, and, then, compared the sampled signals with the triangular carrier waves with a frequency of 500 Hz to generate switching signals. The triangular carrier waves of different cells in phase *k* were displaced from each other by $\pi/N_k$. In this way, phase-shifted carrier PWM was fulfilled [31]. DEWE-2600 data acquisition instrument was used to record the waveforms of the inverter phase voltages ($u_{ag}, u_{bg}$, and $u_{cg}$); the dc voltages of the cells A5, B5 and C5; and the load currents ($i_a, i_b$, and $i_c$). The sampling frequency was 1 MHz. A low-pass filter with a cut-off frequency of 300 kHz was used in the DEWE-2600. Important parameters are listed in Table II.

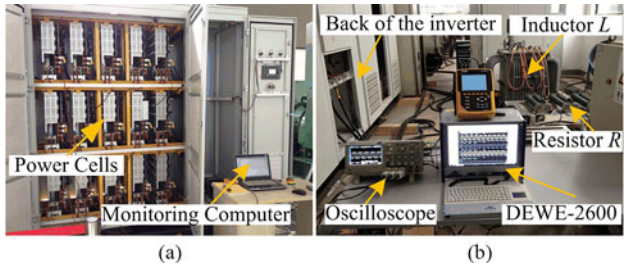


Fig. 11. Pictures of the experimental platform. (a) CHB inverter. (b) Load and the measuring equipment.

TABLE II
MAIN EXPERIMENTAL PARAMETERS

| Parameters | VALUES |
|---|---|
| Normal cells in phase A, B, and C: $(N_a, N_b, N_c)$ | (5, 3, 2) |
| Angular frequency of reference voltages: $\omega$ | 50*2*$\pi$ rad/s |
| RMS value of primary line-to-line voltages | 690 ± 69 V |
| The voltage ratio of the rectifier transformer | 6000 V/705 V |
| DC voltage of each power cell without loads: $V_{\mathrm{dc}1}$ | 109.6 V |
| DC voltage of each power cell with a load: $V_{\mathrm{dc}2}$ | 107.8 V |
| Switching frequency: $f_s$ | 500 Hz |
| Load resistor: *R* | 1.8014 Ω |
| Load induction: *L* | 37.3 mH |
| Proportional coefficient of PI: $K_P$ | 100 |
| Integration coefficient of *P*: $K_I$ | 0.1 |

The method in [22], namely generating $u_0$ by (12), was used as the representative of conventional methods. This method was compared with the proposed OC-ZS control method. The experiments included two parts: Experiment A and Experiment B. Experiment A was performed without any load, so the dc voltage was not affected by load currents. Thus, the output voltages produced by the two methods could be compared under the same condition of $U_{\mathrm{dc}k}$. In Experiment A, we evaluated the ability of the two methods in terms of suppressing BFRP according to the fundamental component of the zero-sequence voltage. Experiment B was performed with the inverter driving a load, as shown in Fig. 1. In this experiment, we compared the

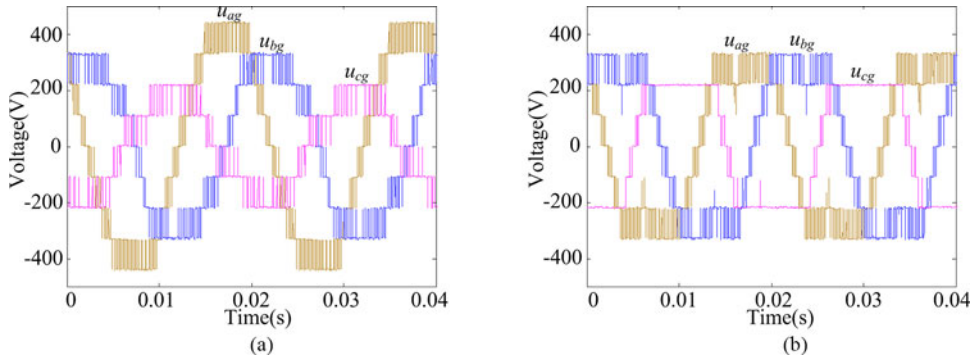


Fig. 12. Inverter phase voltages in Experiment A. (a) Conventional method. (b) Proposed method.

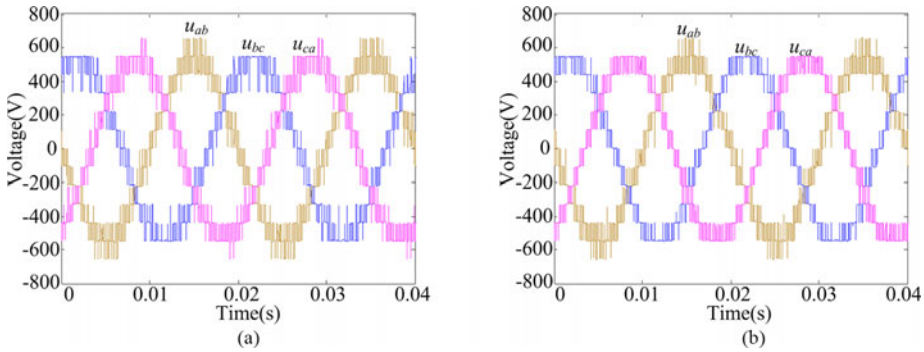


Fig. 13. Line-to-line voltages in Experiment A. (a) Conventional method. (b) Proposed method.

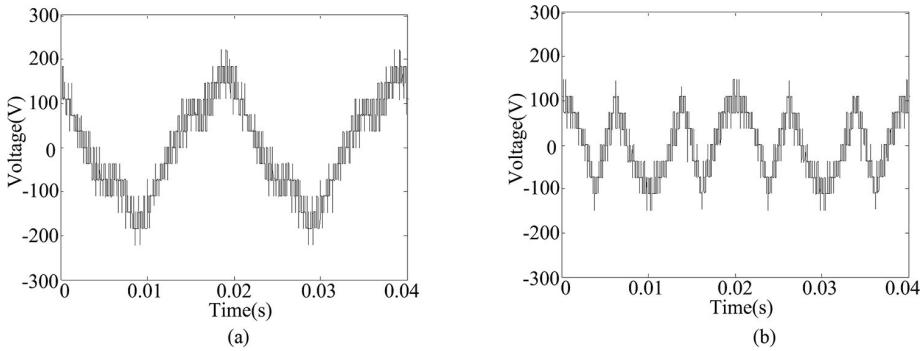


Fig. 14. Zero-sequence voltages in Experiment A. (a) Conventional method. (b) Proposed method.

practical effects of the two methods on suppressing BFRP by observing the rise of the dc voltages.

In the experiments, $(N_a, N_b, N_c) = (5, 3, 2)$. In phase *a*, no cells were bypassed; in phase *b*, cells B1 and B2 were bypassed; in phase *c*, cells C1, C2, and C3 were bypassed.

### A. Experiment A

In this experiment, there were no loads and the dc voltage of each power cell was 109.6 V. Therefore, $U_{\mathrm{dc,min}} = N_c \times 109.6\mathrm{V} = 219.2\mathrm{V}$ and $U_{\mathrm{dc,mid}} = N_b \times 109.6\mathrm{V} = 328.8\mathrm{V}$. According to (11), $U_{\mathrm{MAX}} = 316.4\mathrm{V}$. Thus, we set $U_{m,\mathrm{phase}}$ to 316.4 V to see if the two methods can achieve the maximum available output voltage.

At the beginning of Experiment A, the conventional method was used to generate $u_0$. Then, the proposed method was used. In the process, the inverter phase voltages were recorded by the DEWE-2600. The recorded data were imported into MATLAB. The line-to-line voltages were the differences between the inverter phase voltages, and the zero-sequence voltages could be calculated from $u_0 = (u_{ag} + u_{bg} + u_{cg})/3$. Figs. 12–14 show their waveforms.

Through FFT analysis of the waveforms, the amplitude and phase values of the fundamental components in these waveforms were obtained. According to these values, two phasor diagrams were plotted in Fig. 15. It can be seen that both methods achieved line-to-line voltages with an amplitude near $\sqrt{3}U_{\mathrm{MAX}} = 548$ V, namely the maximum amplitude of the line-to-line voltage that

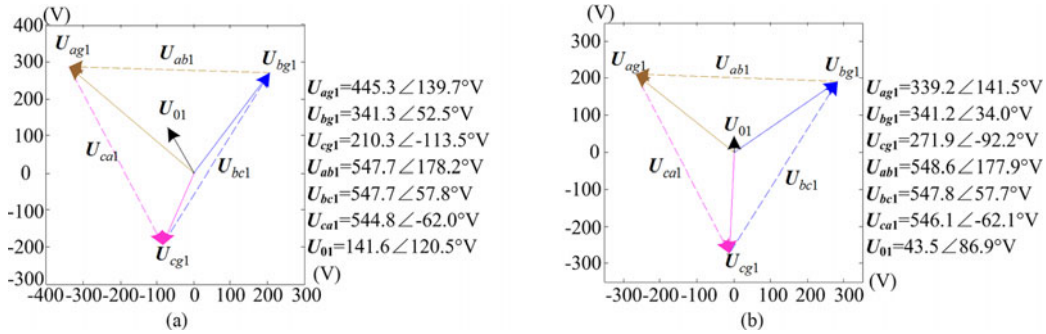


Fig. 15. Phasor diagrams of fundamental components of inverter phase voltages, line-to-line voltages, and zero-sequence voltages in Experiment A. (a) Conventional method. (b) Proposed method.

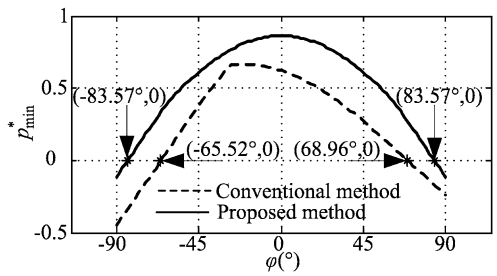


Fig. 16. $p^*_{\min} - \varphi$ curves for the two methods in Experiment A.

can be achieved by linear modulation. This indicates that there are no great differences between the two methods in terms of the output voltage capability.

According to (1), (14), and the data listed in Fig. 15, $\varphi_0$ can be calculated from

$$\varphi_0 = \varphi_{uab} - 30^\circ - \varphi_{u0} \tag{44}$$

where $\varphi_{uab}$ is the phase angle of $\boldsymbol{U}_{\mathrm{ab1}}$; $\varphi_{\mathrm{u0}}$ is the phase angle of $\boldsymbol{U}_{01}$. Substituting the values of $\varphi_{uab}$ and $\varphi_{u0}$ in Fig. 15 into (44), we have $\varphi_0 = 27.7°$ for the conventional method and $\varphi_0 = 60°$ for the proposed method. Substituting the amplitudes of $\boldsymbol{U}_{01}$ in Fig. 15 and $U_{m,\mathrm{phase}} = 316.4$ into (17), we have $U^*_{m01} = 0.4475$ for the conventional method and $U^*_{m,01} = 0.1375$ for the proposed method. Finally, according to (18), (19), $p^*_{\min} - \varphi$ curves for the conventional method and the proposed method are plotted in Fig. 16.

For the proposed method, the range of $\varphi$ satisfying $p^*_{\min} \geq 0$ is $[-83.57°, 83.57°]$; for the conventional method, the range is $[-65.52°, 68.96°]$. Obviously, the allowable range of $\varphi$ for the proposed method is wider than that for the conventional method.

### *B. Experiment B*

In this experiment, a load was connected with the output terminals of the inverter, as shown in Fig. 1. The values of $R$ and $L$ are listed in Table II. The load PF angle was 81.27°. Under such conditions, according to the conclusions in Experiment A, the conventional method will lead to BFRP but the proposed method will not. The dc voltage of each power cell was 107.8 V. Therefore, $U_{\mathrm{dc,min}} = N_c \times 107.8\mathrm{V} = 215.6\mathrm{V}$ and $U_{\mathrm{dc,mid}} = N_b \times 107.8\mathrm{V} = 323.4\,\mathrm{V}$. According to (11), $U_{\mathrm{MAX}} = 311.2\,\mathrm{V}$. Thus, we set $U_{m,\mathrm{phase}}$ to 311.2 V.

First, the proposed method was used to generate $u_0$. Then at time = 1.8 s, the proposed method was dismissed and the conventional method was used. At time = 2.0 s, the conventional method was dismissed and the proposed method was used again. In the process, the inverter phase voltages, the load currents, and the dc voltages of A5, B5, and C5 were recorded by the DEWE-2600. The recorded data were imported into MATLAB and the line-to-line voltages were calculated according to the inverter phase voltages. Fig. 17 shows their waveforms.

It can be seen from Fig. 17 that, once the conventional method was used, the dc voltage of B5 rose drastically. This indicates that the real power flowed back. After the proposed method was used, the dc voltage of B5 recovered gradually. This indicates that the BFRP was suppressed by the proposed method.

Figs. 18–21 show the enlarged waveforms when the conventional method was used and when the proposed method was used. Through FFT analysis of these waveforms, the amplitude and phase values of the fundamental components in these waveforms were obtained. According to these values, two phasor diagrams were plotted in Fig. 22. It can be seen that, when the conventional method was used, the angle between the phasor of the $b$-phase inverter voltage (denoted by $\boldsymbol{U}_{\mathrm{bg1}}$) and the phasor of the $b$-phase load current (denoted by $\boldsymbol{I}_{\mathrm{bg1}}$) was 103.9°, which was greater than 90°; and that when the proposed method was used, the angles between the phasors of the inverter phase voltages and the phasors of the currents in corresponding phases were all less than 90°.

The experimental results suggest that, when $U_{m,\mathrm{phase}} = U_{\mathrm{MAX}}$, the allowable range of $\varphi$ for the proposed method is larger than $[-81.27°, 81.27°]$, which is listed in Table I. On the other hand, the results also show that the allowable range of $\varphi$ for the conventional method is less than $[-81.27°, 81.27°]$ at least when $U_{m,\mathrm{phase}} = U_{\mathrm{MAX}}$. When $U_{m,\mathrm{phase}} < U_{\mathrm{MAX}}$, the region between the waveforms of $u_{\max,s}$ and $u_{\min,s}$ will be wider, so OC-ZS control can suppress the fundamental component of $u_{0,\mathrm{OC-ZS}}$ more effectively. The allowable range of $\varphi$ for the proposed method will also be wider. Therefore, the CRPA of the proposed method is wider than that of the conventional method.

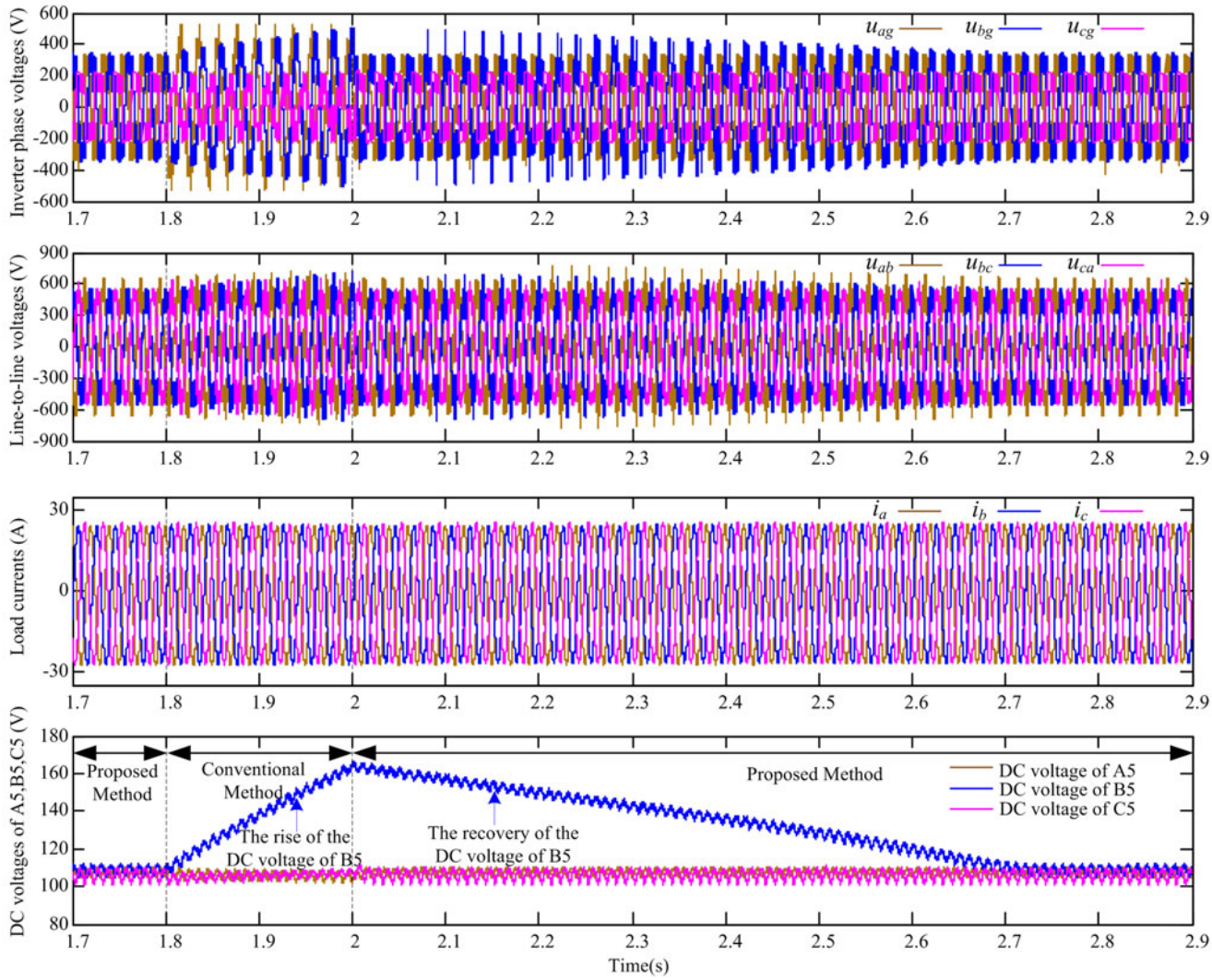


Fig. 17. Global waveforms of inverter phase voltages, line-to-line voltages, load currents, and the dc voltages of A5, B5, and C5 in Experiment B.

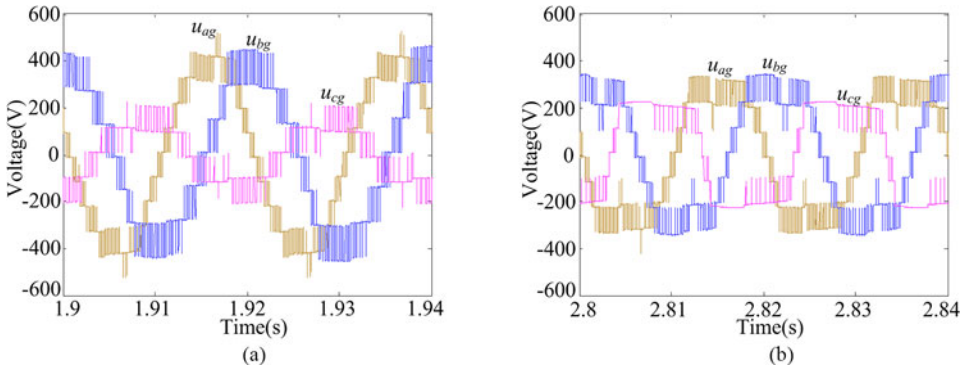


Fig. 18. Enlarged waveforms of the inverter phase voltages in Experiment B. (a) Conventional method. (b) Proposed method.

The two experiments above were performed when $(N_{\max}, N_{\mathrm{mid}}, N_{\min}) = (5, 3, 2)$. However, in the other cases listed in Table I (apart from the cases when $N_{\min} = 0$), it can also be verified by similar experiments or simulations that the CRPA of the proposed method is wider than that of the conventional method. When $N_{\min} = 0$, the CRPA of either the proposed method or the conventional method is $[-60°, 60°]$. Therefore, in general, the proposed method has an obvious advantage over the conventional method in terms of suppressing BFRP.

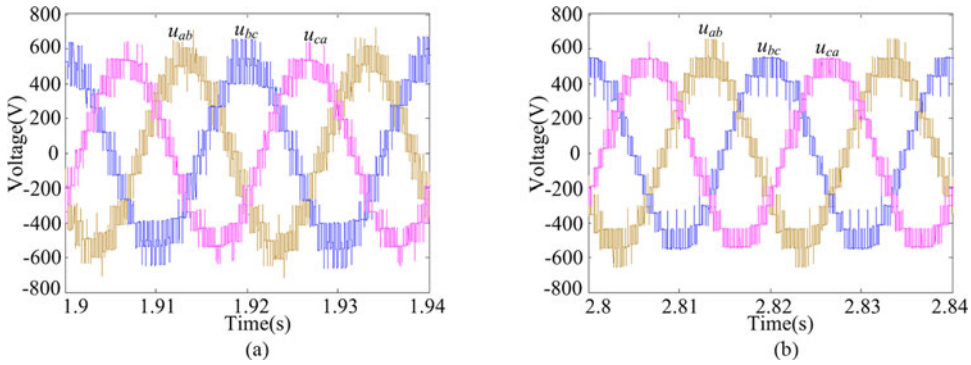


Fig. 19. Enlarged waveforms of the line-to-line voltages in Experiment B. (a) Conventional method. (b) Proposed method.

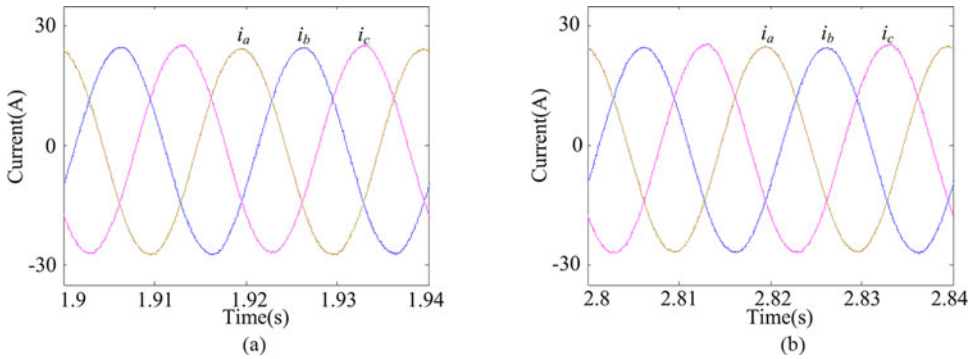


Fig. 20. Enlarged waveforms of the load currents in Experiment B. (a) Conventional method. (b) Proposed method.

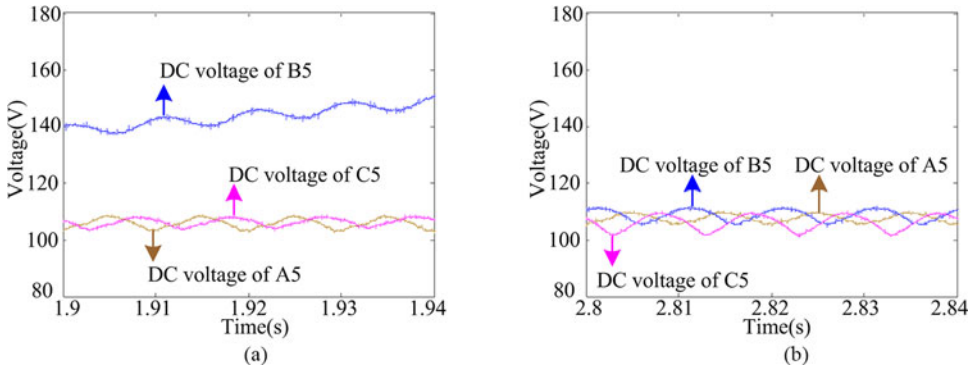


Fig. 21. Enlarged waveforms of the dc voltages of A5, B5, and C5 in Experiment B. (a) Conventional method. (b) Proposed method.

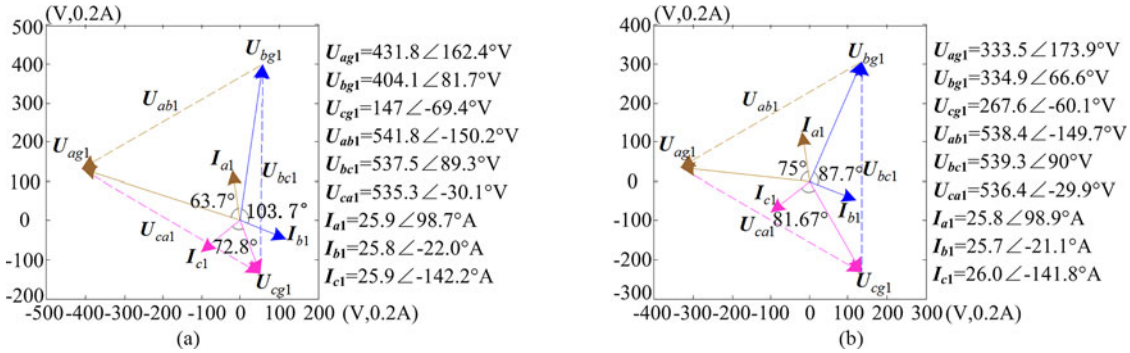


Fig. 22. Phasor diagrams of fundamental components of inverter phase voltages, line-to-line voltages, and load currents in Experiment B. (a) Conventional method. (b) Proposed method.

## V. Conclusion

This paper has made a study of the fault-tolerant control methods based on zero-sequence voltage injection for CHB inverters. To solve the problem of BFRP, to which little attention has been paid so far, we propose a new method called OC-ZS control. The method extends the allowable range of load PF angle without degrading the output voltage capability of the inverter. Compared with the conventional methods, the proposed method enables the CHB inverter to operate in the fault-tolerant mode under a lower load PF without inducing BFRP. As a result, the dc voltage is less likely to rise to an intolerable level and the inverter becomes more reliable.

## References


[1] S. Kouro, M. Malinowski, K. Gopakumar, J. Pou, L. G.Franquelo, B. Wu, J. Rodriguez, M. A. Perez, and J. I. Leon, "Recent advances and industrial applications of multilevel converters," *IEEE Trans. Ind. Electron.*, vol. 57, no. 8, pp. 2523–2580, Aug. 2010.

[2] J. Rodríguez, S. Bernet, B. Wu, J. O. Pontt, and S. Kouro, "Multilevel voltage-source-converter topologies for industrial medium-voltage drives," *IEEE Trans. Ind. Electron.*, vol. 54, no. 6, pp. 2930–2944, Dec. 2007.

[3] A. Das and K. Gopakumar, "A voltage space vector diagram formed by six concentric dodecagons for induction motor drives," *IEEE Trans. Power Electron.*, vol. 25, no. 6, pp. 1480–1487, Jun. 2010.

[4] J. Mathew, P. P. Rajeevan, K. Mathew, N. A. Azeez, and K. Gopakumar, "A multilevel inverter scheme with dodecagonal voltage space vectors based on flying capacitor topology for induction motor drives," *IEEE Trans. Power Electron.*, vol. 28, no. 1, pp. 516–525, Jan. 2013.

[5] C. D. Townsend, T. J. Summers, A. J. Watson, R. E. Betz, and J. C. Clare, "Optimization of switching losses and capacitor voltage ripple using model predictive control of a cascaded H-bridge multilevel STATCOM," *IEEE Trans. Power Electron.*, vol. 28, no. 7, pp. 3077–3086, Jul. 2013.

[6] H. Peng, M. Hagiwara, and H. Akagi, "Modeling and analysis of swithing-ripple voltage on the DC link between a diode rectifier and a modular multilevel cascaded inverter," *IEEE Trans. Power Electron.*, vol. 28, no. 1, pp. 75–84, Jan. 2013.

[7] F. Khoucha, M. S. Lagoun, A. Kheloui, and M. E. H. Benbouzid, "A comparison of symmetrical and asymmetrical three-phase H-bridge multilevel inverter for DTC induction motor drives," *IEEE Trans. Energy Convers.*, vol. 26, no. 1, pp. 64–72, Mar. 2011.

[8] Y. Song and B. Wang, "Survey on reliability of power electronic systems," *IEEE Trans. Power Electron.*, vol. 28, no. 1, pp. 591–604, Jan. 2013.

[9] M. A. Parker, L. Ran, and S. J. Finney, "Distributed control of a fault-tolerant modular multilevel inverter for direct-drive wind turbine grid interfacing," *IEEE Trans. Ind. Electron.*, vol. 60, no. 2, pp. 509–522, Feb. 2013.

[10] L. Sun, Z. Wu, F. Xiao, and X. Cai, "Suppression of real power back flow of non-regenerative cascaded H-bridge inverters operating under faulty conditions," in *Proc. IEEE 6th Energy Convers. Congr. Expo.*, Sep. 2014, pp. 3075–3082.

[11] A. Yazdani, H. Sepahvand, M. L. Crow, and M. Ferdowsi, "Fault detection and mitigation in multilevel converter STATCOMs," *IEEE Trans. Ind. Electron.*, vol. 58, no. 4, pp. 1307–1315, Apr. 2011.

[12] F. Endrejat, R. A. Hanna, and J. Shultz, "Ensuring availability of a large adjustable-speed drive for process gas compressor application rated 11 kV 15.5 MW (20 778 hp)," *IEEE Trans. Ind. Appl.*, vol. 46, no. 5, pp. 1843–1849, Sep./Oct. 2010.

[13] P. Lezana, J. Pou, T. A. Meynard, J. Rodriguez, S. Ceballos, and F. Richardeau, "Survey on fault operation on multilevel inverters," *IEEE Trans. Ind. Electron.*, vol. 57, no. 7, pp. 2207–2218, Jul. 2010.

[14] S. Khomfoi and L. M. Tolbert, "Fault diagnosis and reconfiguration for multilevel inverter drive using AI-based techniques," *IEEE Trans. Ind. Electron.*, vol. 54, no. 6, pp. 2954–2968, Dec. 2007.

[15] P. Lezana, R. Aguilera, and J. Rodriguez, "Fault detection on multicell converter based on output voltage frequency analysis," *IEEE Trans. Ind. Electron.*, vol. 56, no. 6, pp. 2275–2282, Jun. 2009.

[16] W. Song and A. Q. Huang, "Fault-tolerant design and control strategy for cascaded H-bridge multilevel converter-based STATCOM," *IEEE Trans. Ind. Electron.*, vol. 57, no. 8, pp. 2700–2708, Aug. 2010.

[17] P. Lezana, G. Ortiz, and J. Rodriguez, "Operation of regenerative cascade multicell converter under fault condition," in *Proc. 11th Workshop Control Model. Power Electron.*, Aug. 2008, pp. 1–6.

[18] Y. Zang, X. Wang, B. Xu, and J. Liu, "Control method for cascaded H-bridge multilevel inverter failures," in *Proc. 6th World Congr. Intell. Control. Autom.*, Jun. 2006, pp. 8462–8466.

[19] J. Rodriguez, P. W. Hammond, J. Pontt, R. Musalem, P. Lezana, and M. J. Escobar, "Operation of a medium-voltage drive under faulty conditions," *IEEE Trans. Ind. Electron.*, vol. 52, no. 4, pp. 1080–1085, Aug. 2005.

[20] P. Lezana, "Extended operation of cascade multicell converters under fault condition," *IEEE Trans. Ind. Electron.*, vol. 56, no. 7, pp. 2697–2703, Jul. 2009.

[21] P. W. Hammond, "Enhancing the reliability of modular medium-voltage drives," *IEEE Trans. Ind. Electron.*, vol. 49, no. 5, pp. 948–954, Oct. 2002.

[22] F. Carnielutti, H. Pinheiro, and C. Rech, "Generalized carrier-based modulation strategy for cascaded multilevel converters operating under fault conditions," *IEEE Trans. Ind. Electron.*, vol. 59, no. 2, pp. 679–680, Feb. 2012.

[23] Y. Cho, T. L. Bella, J. Lai, and M. K. Senesky, "A carrier-based neutral voltage modulation strategy for multilevel cascaded inverters under unbalanced DC sources," *IEEE Trans. Ind. Electron.*, vol. 61, no. 2, pp. 625–632, Feb. 2014.

[24] P. Lezana, J. Rodriguez, and D. A. Oyarzun, "Cascaded multilevel inverter with regeneration capability and reduced number of switches," *IEEE Trans. Ind. Electron.*, vol. 55, no. 3, pp. 1059–1066, Mar. 2008.

[25] F. Abrahamsen, F. Blaabjerg, J. K. Pedersen, P. Z. Grabowski, and P. Thogersen, "On the energy optimized control of standard and high-efficiency induction motors in CT and HVAC applications," *IEEE Trans. Ind. Appl.*, vol. 34, no. 4, pp. 822–831, Jul./Aug. 1998.

[26] R. E. Betz, T. Summers, and T. Furney, "Symmetry compensation using a H-bridge multilevel STATCOM with zero sequence injection," in *Proc. IEEE 41st Ind. Appl. Conf. Annu. Meet.*, Oct. 2006, pp. 1724–1731.

[27] N. Hatano and T. Ise, "Control scheme of cascaded H-bridge STATCOM using zero-sequence voltage and negative-sequence current," *IEEE Trans. Power Del.*, vol. 25, no. 2, pp. 543–550, Apr. 2010.

[28] L. Maharjan, T. Y. Yamagishi, H. Akagi, and J. Asakura, "Fault-tolerant operation of a battery-energy-storage system based on a multilevel cascade PWM converter with star configuration," *IEEE Trans. Power Electron.*, vol. 25, no. 9, pp. 2386–2396, Sep. 2010.

[29] L. Maharjan, S. Inoue, H. Akagi, J. Asakura, and J. Asakura, "State-of-charge (SOC)-balancing control of a battery energy storage system based on a cascade PWM converter," *IEEE Trans. Power Electron.*, vol. 24, no. 6, pp. 1628–1636, Sep. 2009.

[30] R. Teodorescu, M. Liserre, and P. Rodriguez, *Grid Converters for Photovoltaic and Wind Power Systems*. New York, NY, USA: Wiley, 2011, pp. 74–78.

[31] R. Naderi and A. Rahmati, "Phase-shifted carrier PWM technique for general cascaded inverters," *IEEE Trans. Power Electron.*, vol. 23, no. 3, pp. 1257–1269, May 2009.


**Le Sun** (S'15) was born in Xinjiang, China, in 1987. He received the B.S. and M.S. degrees in electrical engineering from Xi'an Jiaotong University, Xi'an, China, in 2010 and 2012, respectively, where he is currently working toward the Ph.D. degree.

He is a Member at the National Key Laboratory for Vessel Integrated Power System Technology, Naval University of Engineering, Wuhan, China. His research interests include multilevel inverters, modeling of power electronic circuits, and motor control.

**Zhenxing Wu** was born in Hunan, China, in 1982. He received the B.S., M.S., and Ph.D. degrees in electrical engineering from the Huazhong University of Science and Technology, Wuhan, China, in 2004, 2006, and 2010, respectively.

He joined the National Key Laboratory for Vessel Integrated Power System Technology, Naval University of Engineering, Wuhan, China, as a Lecturer, in 2010. His research interests include renewable energy generation, modeling and control of power electronic system, and large-power converters.

**Fei Xiao** was born in China in 1977. He received the B.S. and M.S degrees in electrical engineering from the Naval University of Engineering, Wuhan, China, in 1999 and 2001, respectively. From 2004 to 2012, he was working toward the Ph.D. degree in electrical engineering with Zhejiang University, Hangzhou, China.

From 2003 to 2009, he was a Lecturer with the Naval University of Engineering, Wuhan, China, where he was promoted to an Associate Professor in 2009 and to a Full Professor in 2012. His research interests include renewable energy generation, modeling and control of power electronic system, and high-voltage large-power power electronic equipment.

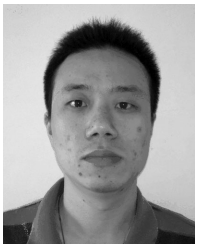

**Xinjian Cai** was born in Fujian, China, in 1979. He received the M.S. degree in control science and engineering from Central South University, Changsha, China, in 2008. He is currently working toward the Ph.D. degree in electrical engineering at the Huazhong University of Science and Technology, Wuhan, China.

He is a Member at the National Key Laboratory for Vessel Integrated Power System Technology, Naval University of Engineering, Wuhan. His research interests include electric drives and power electronics.

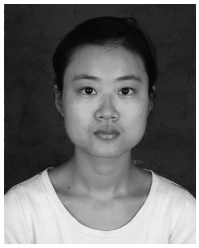

**Shuxiu Wang** was born in Xuzhou, China, in 1990. She received the B.S. degree in electrical engineering from the China University of Mining and Technology, Xuzhou, in 2013. She is currently working toward the M.S. degree at the Naval University of Engineering, Wuhan, China.

Her research interests include multilevel inverters and induction motor drive.